The Astrophysical Journal Letters, 758:L26 (6pp), 2012 October 20 doi:10.1088/2041-8205/758/2/L26
© 2012. The American Astronomical Society. All rights reserved. Printed in the U.S.A.

SLOW MAGNETOACOUSTIC WAVES OBSERVED ABOVE A QUIET-SUN REGION IN A DARK CAVITY

Jiajia Liu[1,3], Zhenjun Zhou[1,3], Yuming Wang[1,4], Rui Liu[1], Bin Wang[2], Chijian Liao[1], Chenglong Shen[1], Huinan Zheng[1], Bin Miao[1], Zhenpeng Su[1], and S. Wang[1]
[1] CAS Key Laboratory of Geospace Environment, Department of Geophysics and Planetary Sciences, University of Science & Technology of China, Hefei, Anhui 230026, China; ymwang@ustc.edu.cn
[2] Beijing Institute of Tracking and Telecommunication Technology, Beijing 100094, China
Received 2012 August 1; accepted 2012 September 14; published 2012 September 27

ABSTRACT

Waves play a crucial role in diagnosing the plasma properties of various structures in the solar corona and coronal heating. Slow magnetoacoustic (MA) waves are one of the important types of magnetohydrodynamic waves. In past decades, numerous slow MA waves were detected above active regions and coronal holes, but were rarely found elsewhere. Here, we investigate a "tornado"-like structure consisting of quasi-periodic streaks within a dark cavity at about 40–110 Mm above a quiet-Sun region on 2011 September 25. Our analysis reveals that these streaks are actually slow MA wave trains. The properties of these wave trains, including phase speed, compression ratio, and kinetic energy density, are similar to those of the reported slow MA waves, except that the period of these waves is about 50 s, much shorter than the typical reported values (3–5 minutes).

Key words: magnetohydrodynamics (MHD) – Sun: activity – Sun: corona – waves

Online-only material: animation, color figures

1. INTRODUCTION

Magnetohydrodynamic (MHD) waves are important phenomena in solar corona and capture broad interests. They are believed to be the energy carriers for coronal heating (e.g., Erdélyi & Fedun 2007; Jess et al. 2009; McIntosh et al. 2011), and a powerful tool to diagnose plasma properties and physical processes in the solar atmosphere (e.g., Roberts 2000; Banerjee et al. 2007; Marsh et al. 2009). Slow magnetoacoustic (MA) waves are one of the eigenmodes of MHD waves, and were frequently observed above the active regions, e.g., in coronal loops, and above coronal holes, e.g., in plumes (e.g., Ofman et al. 1997, 1999; DeForest & Gurman 1998; Berghmans & Clette 1999; Berghmans et al. 2001; Schrijver et al. 1999; Nightingale et al. 1999; De Moortel et al. 2002b; Banerjee et al. 2007; Mariska & Muglach 2010). The propagation speed of these waves is usually around 100 km s^{-1} with a period of about 3 minutes above active regions or about 10–15 minutes above coronal holes. Due to the different magnetic field configurations, they could be found over a wide range of altitudes from 7 Mm to about several hundred megameters above coronal holes (e.g., DeForest & Gurman 1998; Ofman et al. 1997), but usually below 20 Mm in coronal loops above active regions (e.g., Berghmans & Clette 1999; De Moortel et al. 2002a, 2002b).

In past decades, slow MA waves above quiet-Sun regions were rarely reported. This was probably due to the limitations of instruments. Before the era of the *Solar Dynamic Observatory* (*SDO*) mission (Pesnell et al. 2012), imaging instruments provided either full-disk observations at relatively low spatial resolution and low cadence (e.g., *SOHO*/EIT, referring to Delaboudinière et al. 1995; *STEREO*/EUVI, Wuelser et al. 2004), or high resolution and high cadence but limited field of view (FOV; e.g., *TRACE*, Handy et al. 1999; *Hinode*/EIS, Culhane et al. 1997). The AIA instrument (Lemen et al. 2012) on board *SDO* provides the best combination of resolution, cadence, FOV, and EUV wavelength coverage so far. In particular, its full-disk and round-the-clock coverage allow one to launch a comprehensive search for a phenomenon of interest. The only shortcoming of AIA data is the lack of Doppler information. Although this shortcoming adds difficulty to the identification of waves, it could be compensated for by the analysis of multi-wavelength observations. In this Letter, we report an observation of multiple slow MA wave trains in a dark cavity above a quiet-Sun region, which may advance our understanding of MA waves in the solar atmosphere.

2. OVERVIEW

The event of interest took place on 2011 September 25 above the southwest limb within a dark cavity above a quiet-Sun region (as shown in Figure 1(a)). The overall cavity structure stayed stable the entire time, but the prominence-like material under the cavity was perturbed at the beginning of September 25 and finally settled down on the next day. The process from 08:00 to 13:00 UT on September 25 can be seen in the animation associated with Figure 1. Among various phenomena in this process, Li et al. (2012) reported a so-called huge solar tornado.

In this study, we focus on the nature of the repeated quasi-periodic (QP) streaks starting from about 9:00 UT. The clearest group of QP streaks (labeled as S1 in Figure 1(d)) appeared around 10:10 UT in the 171 Å channel, whose peak formation temperature is about 0.63 MK. Several 171 Å images taken before, during, and after this interval are displayed in Figure 1. Before the appearance of the QP streaks, there were apparently two plasma tubes (labeled as 1 and 2) standing right above the limb in the dark cavity (Figure 1(b)). Initially, the two tubes were slightly tangled as if they crossed each other in projection. Thereafter, those two tubes were disturbed by an M1.5 flare in the nearby active region NOAA 11303 (Figure 1(a)) and ended up "apparently" merging together after 9:20 UT.

Meanwhile, continuous upward flows along Tube 1 can be noticed to originate from the tube bottom starting from around 08:20 UT. The upward flows seemingly transformed into

[3] These authors contributed equally to this work.
[4] Corresponding author, ymwang@ustc.edu.cn.

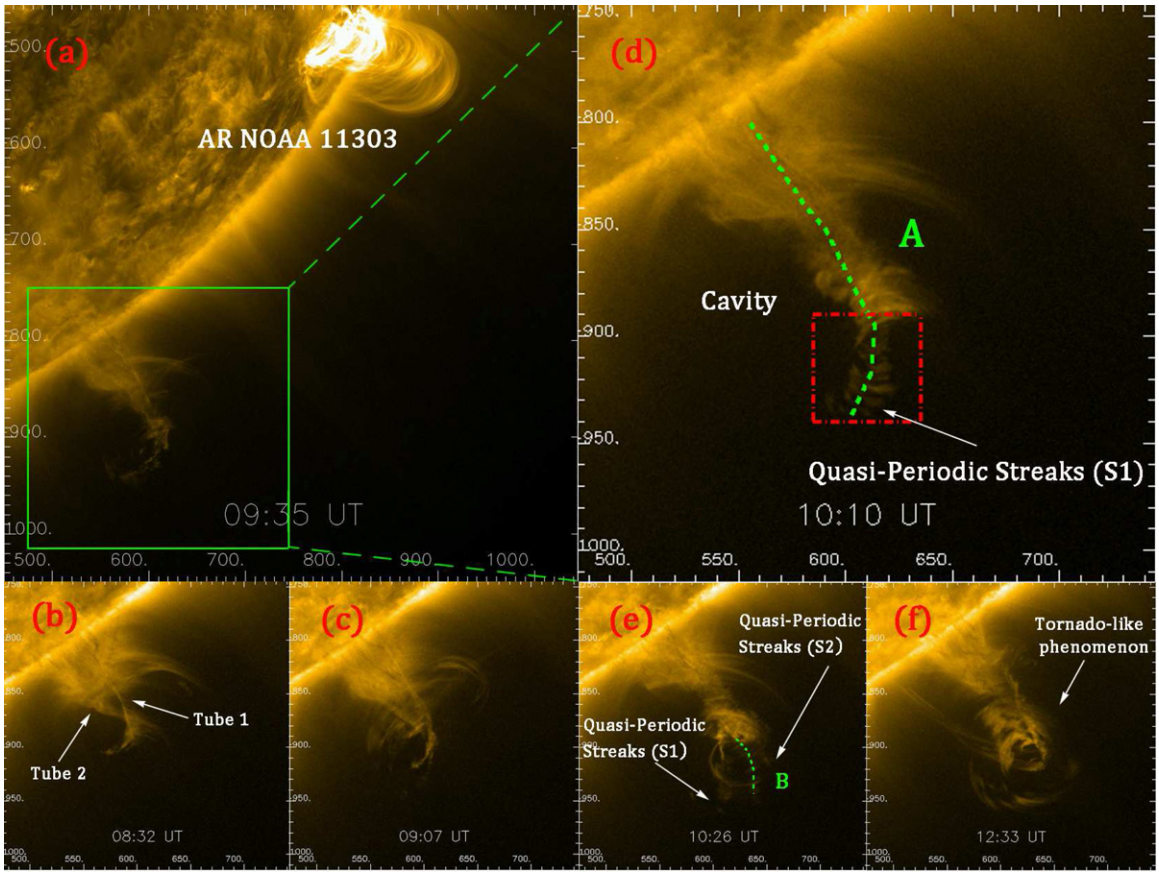

Figure 1. Snapshots taken at the AIA 171 Å passband. The FOV of the image (a) is 600″ × 600″. Images (b)–(f) have the same FOV of 270″ × 270″, which is just the region enclosed by the green box in image (a).
(An animation of this figure is available in the online journal.)

helical-like flows with increasing height, and near the top of Tube 1 the helical-like flows quickly expanded and developed into QP streaks, which intermittently appeared with various intensity and broadness in the next 4 hr. Figure 1(e) shows another group of streaks (labeled as S2). These streaks propagated along the tube once they appeared.

3. HELICAL MAGNETIC STRUCTURE, INTERMITTENT MASS FLOWS, OR WAVE TRAINS?

The nature of the QP streaks is of particular interest. Intuitively, one may think that these QP streaks reflect the helical motion of plasmas in a magnetic flux rope. If this conjecture is true, the degree of the twist of the magnetic field in the flux rope could be inferred from the number of streaks. In the 171 Å image at 10:10 UT, for example, at least 10 streaks were displayed in the upper portion of the tube, and this implies that the magnetic field lines twisted more than 10 rounds or 20π in radians. Previous works have suggested that a flux rope with a force-free field tends to be kink-unstable when the twist exceeds about 3.5π, and the growth rate is on the order of minutes (Hood & Priest 1979; Török & Kliem 2003; Török et al. 2004). Some recent studies further suggested that, for a flux rope with a larger aspect ratio or axial mass flow, the threshold may increase up to 12π (Baty 2001; Srivastava et al. 2010; Zaqarashvili et al. 2010). The QP streaks S1 studied here exceeded the threshold, but did not show any rapid increase in size or brightness or dramatic change in shape, which means that there is no evident signature of the development of kink instability. Moreover, our data process cannot find any signatures of the plasma motion along these streaks. Thus, these QP streaks could not be the result of plasma motion along twisted helical magnetic field lines.

A wave train seems to be a more plausible interpretation for the QP streaks. A 5 pixel wide slice, labeled "A" in Figure 1(d), is placed along the axis of Tube 1 to analyze the plasma motion. Figure 2(a) shows the space–time plot generated by "seeing" through Slice A in AIA 171 Å images. Its left vertical axis gives the distance from the starting point along the slice, and the corresponding height from the solar surface is marked in the right vertical axis. One can see that the lower part of the tube oscillated with a period of about 25 minutes, which was presumably excited by the explosive activity in AR NOAA 11303 at around 09:30 UT (Figure 1(a)). The upward flows mentioned before could be identified as stripes with a positive slope in the plot (Figure 2(a)). Linear fitting to the stripes suggests that the upward flows moved along the tube at a speed of about 32 km s^{-1}.

The QP streaks S1 were located above the distance of 80 Mm after 10:04 UT in Figure 2(a). Figure 2(b) shows a zoom-in plot of the blue box in Figure 2(a) from 10:03 to 10:18 UT. The temporal evolution of these streaks is shown as alternating bright and dark stripes in the space–time plot. Obviously, these stripes are steeper than those produced by the upward flows. According to the space–time plot, the propagation speed of these streaks varied from about 70 km s^{-1} to 120 km s^{-1} with an average speed of about 100 km s^{-1}. It could also be

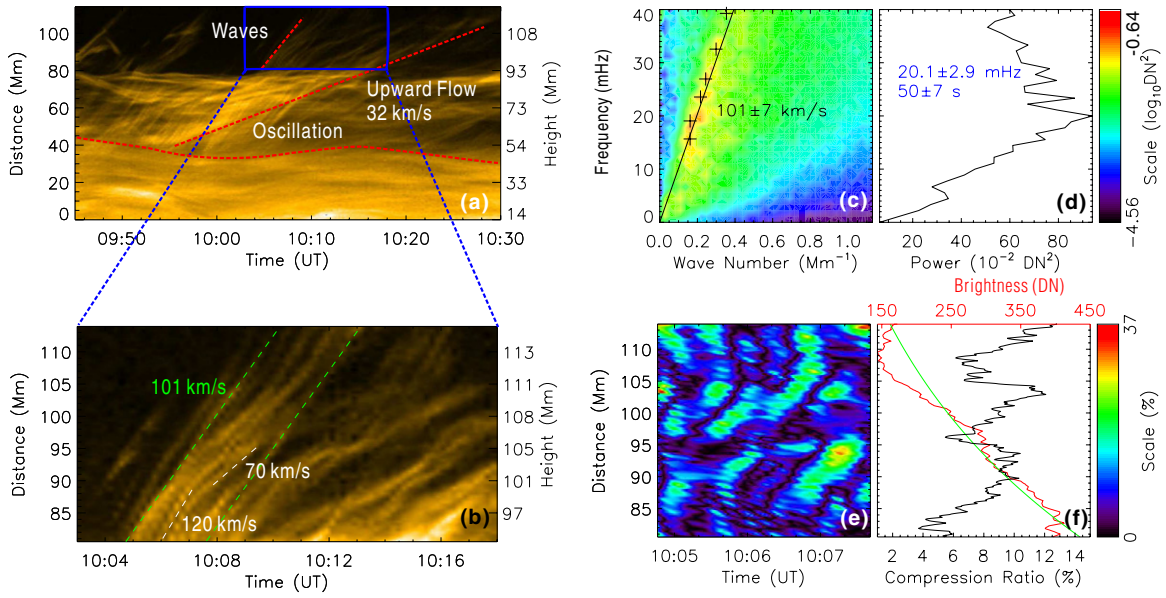

Figure 2. (a) Space–time plot generated along Slice A from AIA 171 Å images with a cadence of 12 s from 09:45 to 10:30 UT. (b) A zoom-in plot of the region enclosed in the blue box in panel (a) from 10:03 to 10:18 UT. (c) Fourier power distribution generated for the 171 Å data enclosed by the red box in Figure 1(d) from 10:03 to 10:18 UT. (d) Integrated power spectrum over wave number of panel (c). (e) Compression ratio in the region between the two green lines in panel (b). (f) Average compression ratio over time of panel (e). The red line shows the averaged brightness over time and the green line is the fitting line.

(A color version of this figure is available in the online journal.)

estimated that the spatial separation of the streaks is about 5 Mm. Therefore, the period is about 50 s if the streaks were caused by a wave train.

Following the method of DeForest (2004) and Liu et al. (2011), Fourier analysis is applied to S1. We generate a three-dimensional data cube using a series of running difference 171 Å images in the FOV enclosed by the red box in Figure 1(d) from 10:03 to 10:18 UT. The Fourier transformation converts the data cube from the space–time domain (x, y, t) to the wavenumber–frequency domain $(k, \omega$; as shown in Figure 2(c)). A slanted stripe with large powers (shown in yellow to red colors) can be clearly seen in Figure 2(c). The phase speed of the wave can be estimated from the slope of the stripe. For that purpose, we equally cut the k–ω plot into six pieces along the frequency axis above 10 mHz, and identify the point with the maximum power in each piece (marked by the plus signs in Figure 2(c)). The phase speed is just the average of the slopes of these points, which is about 101 km s^{-1} with an uncertainty of about 7 km s^{-1}. The integrated power over wave number is presented by the black line in Figure 2(d), which peaks at about 20 ± 3 mHz, corresponding to a period of about 50 ± 7 s. Both results are consistent with the direct estimation from the space–time plot in Figure 2(b).

Performing the same analysis on the QP streaks S2 shown in Figure 1(e), we obtain a similar result which gives a phase speed of about 110 km s^{-1} and a period of about 45 s. These waves were probably excited by the oscillation of the tubes or by upward flows from the tube bottom.

Recently, some researchers have argued that such QP streaks can also be explained by heated QP mass flows (e.g., De Pontieu & McIntosh 2010; McIntosh et al. 2010; De Pontieu et al. 2011; Tian et al. 2011). Those QP mass flows may propagate into the corona at a speed of order 100 km s^{-1}. To distinguish a wave train from QP mass flows, we compare the multi-wavelength observations from AIA as in Kiddie et al. (2012). If the observed QP streaks were produced by mass flows, their propagation

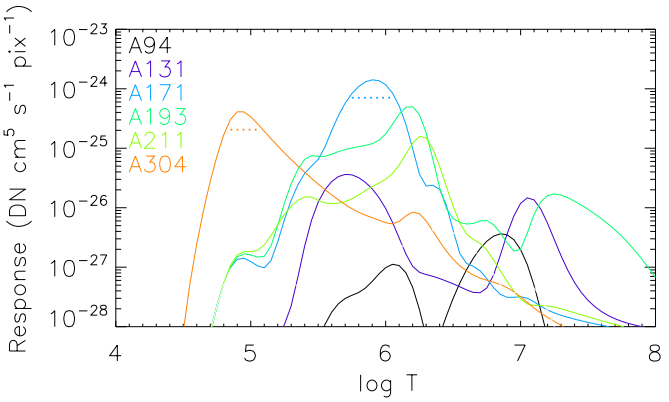

Figure 3. Temperature response curves of AIA passbands. The horizontal dashed lines give the FWHM for 171 Å and 304 Å passbands.

(A color version of this figure is available in the online journal.)

speed would not depend on the temperature, i.e., there would be no dispersion signature; otherwise, the observed QP streaks were caused by an MA wave train.

The temperature response curves of AIA passbands shown in Figure 3, which is generated by the SSW procedure "aia_get_response.pro" provided by the AIA team (Lemen et al. 2012), suggest that, except for 171 Å and 304 Å passbands, all the other passbands obviously correspond to multiple temperatures. Thus, 304 Å data is compared with 171 Å data. It is obvious that there is a similar wave signature in 304 Å data (Figures 4(a) and (b)), and even more importantly, the phase speed is about 70 ± 24 km s^{-1}, which is much smaller than the phase speed derived from 171 Å data. However, there is no clear peak frequency in the integrated power spectrum (Figure 4(c)); the power roughly stays at the same high level from 20 to 40 mHz. This is probably due to the relatively low signal-to-noise in 304 A data. Further, a comparison of the wave phase

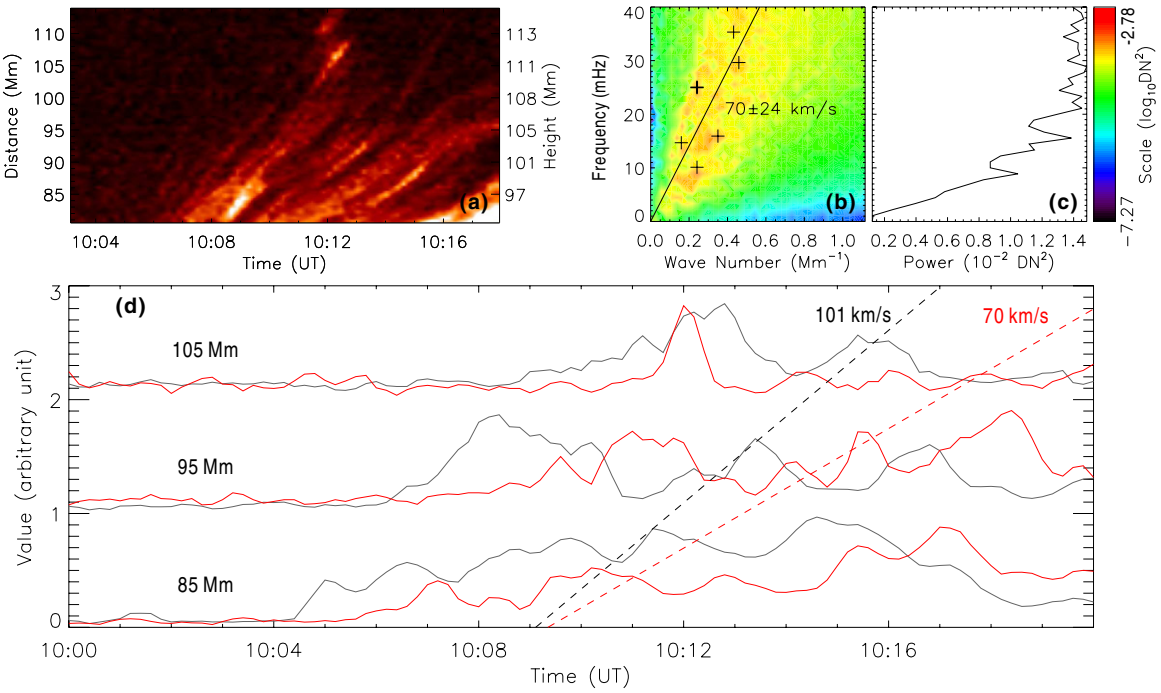

Figure 4. (a)–(c) The same as Figures 2(b)–(d), but for the 304 Å passband. (d) Time sequences at distance 85, 95, and 105 Mm. The black line is for the 171 Å data, and the red line is for 304 Å data. The dashed lines guide the propagation of the same phase.

between the 171 Å and 304 Å data is given in Figure 4(d), in which the time sequences at lower, middle, and higher positions are presented. The phase difference between the two passbands varies with the position changing, which means that the group of QP streaks S1 is likely a wave train rather than mass flows. The dispersion of the MA wave suggests that the plasma tube is likely a multi-thread structure, different threads have different temperatures, and the propagation with different phase speeds in different passbands is equivalent to the propagation of waves in different threads.

4. EVIDENCE OF SLOW MAGNETOACOUSTIC WAVES

The QP streaks as viewed in EUV 171 Å reflect the fluctuation of the emission intensity (i.e., brightness), and therefore the fluctuation of the plasma density. This suggests that these waves are compressional. In order to obtain the amplitude or compression ratio of the wave train S1, the parallelogram defined by the two green dashed lines in Figure 2(b), where the QP streaks are clearest, is further investigated. The background (or unperturbed) brightness in this region is a function of distance, which is obtained by simply averaging the pixel values at each distance, as this region covers several wavelengths of the wave. The red line in Figure 2(f) shows the background brightness, I. The amplitude of the fluctuation of the emission intensity, dI, is therefore obtained by subtracting the background brightness from the observed one. In optically thin corona, it is usually true that $I \propto \rho^2$ and therefore the compression ratio, which is defined as $|d\rho/\rho|$, could be approximately given by $|dI/2I|$ (Aschwanden 2004; Liu et al. 2011).

Figure 2(e) presents the compression ratio in the region of interest. Note that the parallelogram is rectified so that, along the vertical axis, distance and time variations are coupled together. Since the green dashed line is selected to match the wave speed of 101 km s^{-1}, the vertical variation in Figure 2(e) can be roughly interpreted as the variation of the wave amplitude for certain phases. The black line in Figure 2(f) gives the average compression ratio over time, which is about 8.4% on average with a standard deviation of about 2.0%. No significant damping in amplitude is found over the propagation distance of about 33 Mm. Since the amplitude of the density fluctuation is relatively small compared to the background density, it could be treated as a linear wave train. In linear theory, of all propagating MHD waves, only MA waves can cause density compression.

The region we studied is in a dark cavity, presumably void of plasmas (Low 1996; Fuller & Gibson 2009). It is hence expected that the magnetic field inside the dark cavity is relatively stronger than that outside, so that a pressure balance is maintained. Thus the Alfvén speed in the dark cavity should be approximately equal to or even larger than the typical Alfvén speed in a quiet-Sun region, which is about 220 km s^{-1} (McIntosh et al. 2011). The MA waves we investigated here propagated at much slower speeds than the Alfvén speed, and therefore these waves are slow MA waves.

Since these slow MA waves propagated along the tubes, which implies that the wave vector is approximately parallel to the magnetic field lines, the phase speed of the waves should be close to the sound speed. The local sound speed is given by $c_s = \sqrt{2\gamma kT/m}$, where γ is the capacity ratio, k is the Boltzmann constant, m is the proton mass, and T is the temperature. The 171 Å passband corresponds to a temperature of about 0.56–1.1 MK, as indicated by the horizontal dashed line in Figure 3. The sound speed at this temperature range is about 124–176 km s^{-1}. The 304 Å passband corresponds to a temperature of about 0.07–0.11 MK, and the sound speed is about 44–56 km s^{-1}. These results are close to the phase speeds directly derived from the imaging data, but not a perfect

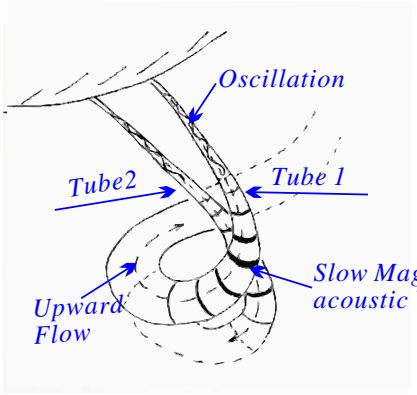

Figure 5. Overview of the 2011 September 25 event.
(A color version of this figure is available in the online journal.)

match, especially for the 171 Å data. There could be various explanations for the deviation. In a uniform magnetic field, if the wave vector of S1 was not exactly parallel to the magnetic field, the phase speed should be smaller than the local sound speed. A projection effect also can result in the underestimation of the derived phase speed from the imaging data. Besides, previous theoretical analysis showed that, in a magnetic tube, slow MA waves propagate at a so-called tube speed, which is smaller than the local sound speed (e.g., Edwin & Roberts 1983).

5. ENERGY FLUX CARRIED BY THE WAVES

The kinetic energy density of an MA wave can be estimated by the formula $\varepsilon = (1/2)\rho v_{\rm ph}^2 (d\rho/\rho)^2$, where ρ is the plasma density and $v_{\rm ph}$ is the phase speed of the wave. The energy flux is given by $F = \varepsilon v_{\rm ph}$. The analysis of the 171 Å data in the previous sections has revealed that for wave S1, $v_{\rm ph}$ is 101 ± 7 km s^{-1} and $d\rho/\rho$ is $8.4\% \pm 2.0\%$. By further assuming the number density to be the typical value of 10^8 cm^{-3} in dark cavities (Fuller & Gibson 2009), we infer that the energy density carried by wave S1 is $3.0 \times 10^{-5} \sim 1.2 \times 10^{-4}$ erg cm^{-3}, or the energy flux is $2.8 \times 10^2 \sim 1.1 \times 10^3$ erg cm^{-2} s^{-1}.

Since the emission intensity, and therefore the density, obviously decreases with increasing distance (Figure 2(f)), the wave energy actually dissipated when it propagated along the tube. We applied an exponential equation $I(x) = ae^{c(x-b)}$ to fit the observed brightness given by the red line in Figure 2(f). The free parameters a, b, and c are found to be 434, -0.03, and 80, respectively. The green fitting curve suggests that the background brightness weakened by a factor of 63% over a distance of about 33 Mm or in about 5 minutes. Thus, it is inferred that the average dissipation rate of the wave energy is $3.9 \times 10^{-8} \sim 1.6 \times 10^{-7}$ erg cm^{-3} s^{-1}.

6. SUMMARY

In this Letter, we identified the QP streaks, appearing above a quiet-Sun region on 2011 September 25, with slow MA waves. The overall picture of this "tornado"-like event is summarized in Figure 5. There were two flux tubes in a dark cavity. Oscillations and upward flows were initiated in the tubes around 08:00 UT by some perturbations. About one hour later, slow MA waves were excited by the oscillations and/or the upward flows, and manifested as QP streaks in the upper portion of the tubes. The tornado-like phenomenon shown in Figure 1(f) was the result of bulk flows along the curved tubes.

The wave train S1 propagated along Tube 1 around 10:10 UT is particularly analyzed. Its propagation speed is about 101 km s^{-1} in the 171 Å passband or 70 km s^{-1} in the 304 Å passband, which is comparable with those of the slow MA waves found above active regions, 122 km s^{-1} (De Moortel et al. 2002a, 2002b) or coronal holes, 75–150 km s^{-1} (DeForest & Gurman 1998), while its period is about 50 s, which is much shorter than those found above active regions, ~3 minutes, or coronal holes, usually 10–15 minutes. According to the fluctuation in brightness, the density amplitude of the wave is about 8.4%, also comparable with that of the slow MA waves found elsewhere (~4% above active regions and 10%–20% above coronal holes, respectively). The dissipation rate of the wave energy is estimated from 3.9×10^{-8} to 1.6×10^{-7} erg cm^{-3} s^{-1}, which is about one order of magnitude smaller than that of the radiative loss of the local corona (Withbroe & Noyes 1977; Aschwanden 2006).

Our study implies that (1) slow MA waves not only appear above active regions or coronal holes but also exist above quiet-Sun regions, and the fact that they were rarely found above quiet-Sun regions before the *SDO* mission is probably simply due to instrument limitation and (2) the slow MA wave train in this study is not sufficient for local coronal heating. It should be noted that slow MA waves were repeatedly observed during the event, and sometimes two or more wave trains appeared simultaneously. Whether such slow MA waves ubiquitously exist in the corona and whether they make a significant contribution to coronal heating is worth investigating further.

We acknowledge the use of data from the AIA instrument on the *Solar Dynamics Observatory*. This work is supported by grants from the CAS (the Key Research Program KZZD-EW-01-4, 100-talent program, KZCX2-YW-QN511 and startup fund), 973 key project (2011CB811403), NSFC (41131065, 40904046, 40874075, and 41121003), MOEC (20113402110001), and the fundamental research funds for the central universities.

REFERENCES

Aschwanden, M. J. 2004, in Proc. of the SOHO 15 Workshop—Coronal Heating, ed. R. W. Walsh, J. Ireland, D. Danesy, & B. Fleck (ESA SP-575; Paris: ESA), 97
Aschwanden, M. J. 2006, Physics of the Solar Corona - An Introduction with Problems and Solutions (Berlin: Springer)
Banerjee, D., Erdélyi, R., Oliver, R., & O'Shea, E. 2007, Sol. Phys., 246, 3
Baty, H. 2001, A&A, 367, 321
Berghmans, D., & Clette, F. 1999, Sol. Phys., 186, 207
Berghmans, D., Mckenzie, D., & Clette, F. 2001, A&A, 369, 291
Culhane, J. L., Harra, L. K., James, A. M., et al. 1997, Sol. Phys., 243, 19
De Moortel, I., Hood, A. W., Ireland, J., & Walsh, R. W. 2002a, Sol. Phys., 209, 89
De Moortel, I., Ireland, J., Walsh, R. W., & Hood, A. W. 2002b, Sol. Phys., 209, 61
De Pontieu, B., & McIntosh, S. W. 2010, ApJ, 722, 1013
De Pontieu, B., McIntosh, S. W., Carlsson, M., et al. 2011, Science, 331, 55
DeForest, C. E. 2004, ApJ, 617, L89
DeForest, C. E., & Gurman, J. B. 1998, ApJ, 501, L217
Delaboudinière, J.-P., Artzner, G. E., Brunaud, J., et al. 1995, Sol. Phys., 162, 291
Edwin, P. M., & Roberts, B. 1983, Sol. Phys., 88, 179
Erdélyi, R., & Fedun, V. 2007, Science, 318, 1572
Fuller, J., & Gibson, S. E. 2009, ApJ, 700, 1205
Handy, B. N., Acton, L. W., Kankelborg, C. C., et al. 1999, Sol. Phys., 187, 229
Hood, A. W., & Priest, E. R. 1979, A&A, 77, 233
Jess, D. B., Mathioudakis, M., Erdélyi, R., et al. 2009, Science, 323, 1582
Kiddie, G., De Moortel, I., Del Zanna, G., McIntosh, S., & Whittaker, I. 2012, Sol. Phys., 279, 427

Lemen, J. R., Title, A. M., Akin, D. J., et al. 2012, Sol. Phys., 275, 17
Li, X., Morgan, H., Leonard, D., & Jeska, L. 2012, ApJ, 752, L22
Liu, W., Title, A. M., Zhao, J. W., et al. 2011, ApJ, 763, L13
Low, B. C. 1996, Sol. Phys., 167, 217
Mariska, J. T., & Muglach, K. 2010, ApJ, 713, 573
Marsh, M. S., Walsh, R. W., & Plunkett, S. 2009, ApJ, 679, 1674
McIntosh, S. W., Innes, D. E., De Pontieu, B., & Leamon, R. J. 2010, A&A, 510, L2
McIntosh, S. W., Pontieu, B. D., Carlsson, M., et al. 2011, Nature, 475, 477
Nightingale, R., Aschwanden, M., & Hurlburt, N. E. 1999, Sol. Phys., 190, 249
Ofman, L., Nakariakov, V., & DeForest, C. E. 1999, ApJ, 514, 441
Ofman, L., Romoli, M., Poletto, G., Noci, G., & Kohl, J. L. 1997, ApJ, 491, L111
Pesnell, W. D., Thompson, B. J., & Chamberlin, P. C. 2012, Sol. Phys., 275, 3
Roberts, B. 2000, Sol. Phys., 193, 139
Schrijver, C. J., Title, A. M., & Berger, T. E. 1999, Sol. Phys., 187, 261
Srivastava, A. K., Zaqarashvili, T. V., Kumar, P., & Khodachenko, M. L. 2010, ApJ, 715, 292
Tian, H., McIntosh, S. W., & De Pontieu, B. 2011, ApJ, 727, L37
Török, T., & Kliem, B. 2003, A&A, 406, 1043
Török, T., Kliem, B., & Titov, V. S. 2004, A&A, 413, L27
Withbroe, G. L., & Noyes, R. W. 1977, ARA&A, 15, 363
Wuelser, J.-P., Lemen, J. R., Tarbell, T. D., et al. 2004, Proc. SPIE, 5171, 111
Zaqarashvili, T. V., Díaz, A. J., Oliver, R., & Ballester, J. L. 2010, A&A, 516, A84